ACOUSTICAL EFFECTS OF INTERNAL TIDES ON SHALLOW WATER PROPAGATION : AN OVERVIEW OF THE INTIMATE96 EXPERIMENT

Y. Stéphan, X. Démoulin
Centre Militaire d'Océanographie
EPSHOM, BP426
29275 Brest Cedex, FRANCE

T. Folégot
ATLANTIDE
Technopole Brest Iroise, Site du Vernis
29608 Brest Cedex, France

S.M. Jesus
UCEH, Universidade do Algarve
Campus de Gambelas
8000 Faro, PORTUGAL

M. B. Porter
Ocean Sciences Division
Science Applications International Corporation
10260 Campus Point Drive
San Diego, CA 92212-1578, USA

E. Coelho
Instituto Hidrografico,
Ruas das Trinas, 49
1296 Lisbon, PORTUGAL

Abstract

This paper presents an overview of the experiment INTIMATE96, carried out in June 1996 on the continental shelf off the coast of Portugal and discusses the effects of internal tides on the acoustic propagation. A towed broadband acoustic source and a 4-hydrophone vertical array were used. Acoustic data were collected for 5 days, including legs where the source ship was moving and legs with the ship on station. Intensive environmental surveys (XBT, CDT, bottom and hull-mounted ADCP, thermistor chain, bathymetry, geoacoustic characteristics of the sediments) were also conducted. The central

results of acoustic data processing is that several effects of the environment, including bottom influence, source range and depth and internal tides effects, can be clearly seen on the signals and they can be processed separately. The acoustical effect of tides enables to perform inversion with simple and fast methods. The results of INTIMATE96 confirm the efficiency of broadband analysis on a single hydrophone to infer the geophysical environment.

1. Introduction

Internal tides are internal waves at tidal frequencies induced by the interaction between the astronomic tide and the topography (e.g. [1]). In density-stratified seas, the barotropic forcing, combined with the topography gradients, generates internal waves, that travel away from the generation point. In particular, continental shelf-breaks create two main internal tides waveforms, propagating in both the deep and the shallow ocean. Internal tides and internal waves are interesting for two main purposes. First, internal tides have recently renewed their importance for oceanographers as a mean of understanding how the ocean dissipates the lunar energy [2]. The internal tide appears to be a key link in the cascade of energy from the large to the small scale. Second, because of their influence on acoustic propagation, internal tides have also aroused the interest of acousticians for many years (e.g. [3,4]). The recent development of ocean acoustic tomography [5] has reinforced the interest for acoustical imaging of internal tides. On the one hand, the inversion of tomographic signals allows for the observation and characterization of barotropic and baroclinic internal tides modes [6]. On the other hand, the analysis of propagated signal gives an idea of the acoustical impact of internal tides and internal waves (e.g. [7,8]), especially in shallow water.

In the past, many experimental and theoretical studies were carried out to understand and model the mechanisms of internal tides generation and propagation (e.g. [9,10,11]). A strong interest has been devoted to the continental slope along the coasts of the North-East Atlantic (Celtic, Armorican and Iberian shelves), known to be at the origin of strong internal tides and internal waves [12, 13, 14]. A previous tomography experiment, called GASTOM90, was conducted by the French Hydrographic and Oceanographic Office (SHOM) in the bay of Biscay. This experiment had already shown the strong influence of internal tide on long-range acoustic propagation [15,16]. On this basis, enforced by the emerging interest towards shallow water tomography, a joint project was build between SHOM, the Hydrographic Institute of Portugal (IH), the University of Algarve (UAL) and the New Jersey Institute of Technology (NJIT). The so-called INTIMATE project (INternal Tide Investigation by Means of Acoustic Tomography Experiment) is a series of experiments specifically designed to tomographically image internal tides at a basin scale.

The first exploratory experiment was carried out in June 1996 on the continental shelf off the coast of Portugal [17]. This experiment, which was the first underwater acoustic experiment in Portugal, aimed to collect a shallow water data set to check the feasibility of internal tide imaging in a coastal environment. A towed broadband acoustic source and a 4-hydrophone vertical array were used. Acoustic data were collected for 5 days,

including legs where the source ship was moving and legs with the ship on station. Intensive environmental surveys (XBT, CDT, bottom and hull- mounted ADCP, thermistor chain, bathymetry, geoacoustic characteristics of the sediments) were also conducted. This paper presents an overview of the experiment and discusses the effects of internal tides on the acoustic propagation.

The paper is organized as follows. Section 2 gives an overview of the experiment and describes the main features of acoustic propagation in the observed environment. Section 3 presents the influence of the tide on the acoustic propagation by isolating the effect of each mode. Section 4 presents the acoustic data inversion and discusses the tomographic imaging of two internal tidal cycles. Conclusions and perspectives are drawn at the end of the paper.

2. The INTIMATE 96 experiment

2.1. GENERAL DESCRIPTION AND STRATEGY

The INTIMATE96 experiment was carried out in the period of 10-19 June in the Nazaré site, on the continental shelf, 50 nautical miles north of Lisbon (figure 1). This area is in the vicinity of the shelf break, favorable to the generation of internal tides. To complete the knowledge of the area, additional bathymetric surveys were carried out and a seismic survey combined with cores and samplings were also conducted [18], reavealing a smooth and sandy bottom.

The experiment consisted in acoustic transmissions between a broadband source (towed by the French oceanographic vessel BO D'Entrecasteaux) and a 4-hydrophone array (figure 2). Hydrophones were located at 35, 70, 105 and 115 meters. Near the array were also moored a thermistor chain and a Doppler current profiler. The signals received on the hydrophones were transmitted and processed aboard the Portuguese hydrographic vessel NRP Andromeda for real time analysis. Three acoustic phases were carried out (figure 3):

- Station «NORTH»: This phase consisted in a 25-hour acoustic station 5.6 km north from the hydrophone array. The purpose of the station was to collect data in a range independent environment. Acoustic signals propagate on a flat bottom along an isophase line of the internal tide. During the station, CTD and XBT profiles were made every 2 hours respectively by NRP Andromeda near the array and by BO D'Entrecasteaux at the station point.

- «TRACKING»: This phase consisted in a 10-hour acoustic leg with a moving source. The purpose of this phase was to collect data in various environmental configurations (source depth, propagation range and bathymetric variations). CTD profiles were made by NRP Andromeda near the array and XBT launches were performed by BO D'Entrecasteaux along the acoustic tracks (bathymetric profiles were also done with a 50m spatial resolution).

- Station «WEST»: 25-hour acoustic station 6.8 kilometers west of the hydrophone array. The purpose of this station was to collect data along range-dependent sections and with a direction of acoustic propagation across the isophase lines of the internal tide. During

the station, CTD and XBT profiles were done every 2 hours respectively by NRP Andromeda near the array and BO D'Entrecasteaux at the station point.

2.2. ACOUSTIC DATA

The emitted signal was a 300-800 Hz LFM chirp. The chirp lasted for 2 seconds and was emitted every 8 seconds. Each received sequence was cross-correlated with the emitted signal. Finally, all sequences were lined up on the leading edge. The sampling rate is 1 ms. The images of acoustic recordings during the three phases on hydrophone 1 (35 meters) and hydrophone 3 (115 meters) are presented in figure 4. The amplitudes are normalized respect to the maximum value of the first spike on each image (the dB scales is up to zero). The subplots shows that the signals have a stable part composed of separated arrivals. This stable part looks like a textbook multipath pattern. Notice that during the stations, the arrival times of the rays varies with an M2 cycle (two cycles per day). Also, during the tracking phase, the structure changes significantly as the source moves to and from the array. Finally, the energy of the first spike has large fluctuations. This is the unstable part of the signal.

2.3. DATA INTERPRETATION

2.3.1. Background environment
The sound speed profiles collected during the experiment exhibit a smooth downward refracting gradient, with no significant mixed layer (figure 5, top). A series of temperature profiles obtained by the thermistor chain near the vertical array is given in figure 5, bottom. It shows that the thermocline oscillates between 30 and 70 meters with a typical M2 cycle (two cycles in 25 hours). High frequency oscillations can also be observed.

2.3.2. Influence of the sound speed profile
Acoustic simulations have been carried out using a ray tracing model to describe the geometry of rays and the KRAKEN normal mode program [19] to study the impulse response of the medium. The bottom is flat and sandy with a compressional speed of 1700 m/s and attenuation coefficient of 0.9 dB/λ. The propagation of broadband signals in the INTIMATE96 shallow water environment can be characterized by two regimes (figure 6): a stable regime and an unstable regime.

This unstable part is composed of direct rays refracted in the thermocline or with only a few surface or bottom reflections. This leads to the existence of a first spike. The amplitude of this spike is expected to be sensitive to the depth and gradient of the thermocline since it results from the combination of several rays refracted in the thermocline. Any fluctuation of this thermocline is expected to modify the interference scheme and so the amplitude of the spike.

The second part of the signal is very stable and is composed of surface and bottom reflected rays (or equivalently modes interacting with both the boundaries). These paths sweep the complete water column. The arrival times of such rays are expected to be sensitive to two features. First, the external tides, which modify the water depth, affect the paths lengths and, consequently, the travel times. Second, the internal tide modifies the

mean value of the sound speed over the water column since the thermocline goes up and down. Hence, the travel times, which depend on this mean value, should also be affected. This sensitivity will be discussed later on.

3. Acoustical effects of tides

The fluctuation of the sound speed profiles can be represented by two families of normal modes. The first one, the family of Empirical Orthogonal Functions (EOF), is computed from the covariance matrix of the profile. Thus, it captures the ocean variability. The second set, the dynamical modes, is computed from the mean density profile and is closely related to the physical process of internal tides. In the INTIMATE96 experiment, it is remarkable that the two sets are almost equivalent [20]. This suggests that the ocean variability observed in the sound speed profile is mainly governed by internal tide effects. Two EOFs, which affects the sound speed profile, are given in figure 7. They are sufficient to represent about 85 % of fluctuations in the thermocline. In the following, these two first modes will be used to interpret the acoustic fluctuations in the data.

3.1. Effect of the surface tide

The barotropic mode represents the sea-surface elevation due to the external tides. The main effect of this mode is that the water depth is periodically increasing and decreasing by a few meters. As a consequence, the path-length of rays reflected at the surface and the bottom shortens and lengthens with the same period. In addition, the more the rays have swept the water column, the more they are sensitive to the water depth. Then, the rays most affected by the barotropic tide are rays with high grazing angles. This explains the fluctuations of late arrivals on the real data as already shown in figure 4. This is also emphasized in figure 8 , which shows an excellent correlation between the predicted tide and the time of arrival of the last rays during station «NORTH». The fluctuation of the differential travel times for last rays is up to 15 ms.

On the other hand, figure 9, top, shows that the travel time of the first rays is not affected by the sea-surface elevation.. For variations up to 10 meters, the travel time remains constant. Indeed, these rays are refracted in the thermocline. Consequently, they are not sensitive to the fact that the surface goes up and down. They are only sensitive to the internal tide as will be discussed in the following. It is important to notice that, as the travel time of direct rays is not modified, inverting the absolute travel times of last rays is equivalent to inverting differential travel times (the difference between the travel time of a ray and the travel time of the leading edge).

It is also shown in figure 9, top that the travel times of bottom-surface reflected rays increases with the sea-surface elevation in a linear way. This was expectable since the length of the paths depends on the surface of the sea. As will be explained later, this effect can be filtered.

3.2. Effect of the internal tide

3.2.1. First baroclinic mode

The first baroclinic mode represents the oscillation of the thermocline. It has two main influences, put forward in figure 9, middle.

The first influence is that the amplitude and width of the first spike are modified when the first mode varies (see the fluctuations vs alpha in the interval 100-200 ms). The explanation lies in the fact that the first mode fluctuation affects the position of the thermocline. As the first arrivals are rays refracted in the thermocline, the energy of the first packet can oscillate.

The second influence is that the mean sound speed value over the water column is modified. The mean value increases when the thermocline deepens. Consequently, the times of arrival of rays sweeping the water column are also modified. The effect is seen on late arrivals (see for instance the rays around 600 ms). The influence on late arrivals is only of a few milliseconds, to be compared to the fluctuations of the same rays with the external tide effect. Note also that the later the ray, the greater the influence. To observe the influence of internal tides, it is preferable to track the time of arrival of the last ray.

3.2.2. Second baroclinic mode

The effect of the second baroclinic mode, well represented by the second EOF, is shown in figure 9, bottom). Two conclusions can be drawn.

First, as for the first mode, the amplitude and width of the first spike are modified when the second mode varies (see the fluctuations vs alpha in the interval 100-200 ms). This is due to the fact that beta represents the shear of the thermocline. Then, it modifies the gradient of thermocline and can affect the energy of the first packet, composed by refracted rays.

Second, the travel time of the late arrivals are unchanged (see for instance the rays around 600 ms and compare with figure 9, middle). This can be explained by the fact that the shear effect does not modify the mean value of the sound speed over the water column.

3.3. Summary

We have seen that the oceanographic fluctuations in the sound speed profile have three main origins: the barotropic tide, which results in fluctuations in the water depth; the first baroclinic mode, which results in fluctuations of the depth of the thermocline; and the second baroclinic mode, which results in fluctuation of the gradient of the thermocline. The influence on the propagated signal is of two types: the barotropic tide as well as the first mode can modify the time of arrival of late rays. The first and second modes modify the energy of the first spike. These different features are clear on the real data and are also well modelled by ray tracing and normal modes codes.

4. Inversion

The purpose of inversion is to retrieve the main caracteristics of the internal tides. These characteristics are the amplitude, the wavelength and the direction of propagation. The first two features can be represented by the coefficient of the first two EOFs. The last one can be estimated by combining the results of the two stations.

4.1. STATEMENT OF THE INVERSE PROBLEM

The evolution of the sound speed profile can be written as the expansion with the first two EOF's:

$$c_1(z, t) = c_0(z) + \alpha(t) \cdot \Psi_1(z) + \beta(t) \cdot \Psi_2(z), \qquad (1)$$

where $c_0(z)$ is the mean sound speed profile, $\alpha(t), \beta(t)$ and $\Psi_1(z), \Psi_2(z)$

are respectively the coefficient and the shape of the first two EOFs.
The inverse problem lies in the estimation of the two-modes coefficient from the time of arrivals of the bottom-surface reflected rays and from the amplitude of the first spike. In practice, using only the differential time of arrival of the last ray is sufficient. Indeed, the last ray is the most sensitive rays and contains all the invertible information necessary to retreive the first mode. Inversion attemps with several rays showed that no improvment

was obtained on $\alpha(t)$ estimate. If we denote respectively by A(t) and τ(t) the amplitude of the first spike and the differential travel time, the inverse problem can be written in its general form as:

$$\begin{bmatrix} \tau(t) \\ A(t) \end{bmatrix} = G(\alpha(t), \beta(t)) , \qquad (2)$$

where G is a non linear operator that will be expressed in two steps.
Indeed, it has been shown in section 3.2.2 that the differential travel times does not depend on the second EOF. Thus, it can be written that:

$$\tau(t) = G_1(\alpha(t)). \qquad (3)$$

Once $\alpha(t)$ is estimated, the relationship between the amplitude and the second EOF can be expressed as:

$$A(t) = G_\alpha(\beta(t)), \qquad (4)$$

It is then possible to define a hierarchical inverse method: in a first step, the first coefficient can be retrieved from the temporal fluctuations of bouncing rays, in a second step, the second coefficient can be obtained by minimizing the mismatch between the mea-

sured and the predicted amplitude of the first spike in a matched-field processing fashion. One difficulty in this approach is to normalize the synthetic data to ensure that the correlation with normalized real data makes sense. This will be explained later on.

4.2. APPLICATION TO ACOUSTIC DATA

4.2.1. Filtering out the barotropic tide
The arrival time of the bottom-reflected rays are sensitive to both the external tide and the internal tide. To exhibit the internal tide signature, it is then necessary to filter the differential travel times out of the effect of the sea surface height. The amplitude of the tide during the INTIMATE96 experiment is about 3 meters. By considering a constant bathymetric gradient, a simple model of the travel time perturbation due to the water depth can be expressed. The complete development of the model is given in [20] and yields :

$$\Delta \tau_i \approx \frac{2hN_i}{c_f} \cdot [\sin \alpha_i^S + N_i \cdot \alpha_b \cdot \cos \alpha_i^S] \ . \tag{5}$$

where α_b is the angle of the bathymetry, $\Delta\tau_i$ is the travel time perturbation of ray i, h is the mean water depth and c_f represents the water sound speed at the bottom, α_i^S is the grazing angle at the source, N_i is the number of bottom reflections. To validate this model, comparisons between the exact travel times computed from standard ray tracing and corrected travel times computed from Eq. (5) have been carried out. The absolute error is less that 0.3 milliseconds, which is consistent with the time resolution on the data (one millisecond). Then, a temporal filter can be applied to the travel time of bouncing rays to filter out the external tide effect.

4.2.2. Inversion of the internal tide signal

a. Inversion of the first mode
The travel time perturbation of the i-th ray is given by:

$$\delta t_i \approx -\int_{\Gamma_i} \frac{\delta c(z)}{c_0(z)^2} d\Gamma \ . \tag{6}$$

The sound speed profile projected on the first mode can be expressed as:

$$c(z, t) = c_o(z) + \alpha(t) \cdot \Psi_1(z) \ . \tag{7}$$

It can be written that:

$$\delta t_i \approx -\alpha \cdot \int_{\Gamma_i} \frac{\Psi_1(z)}{c_0(z)^2} d\Gamma \quad . \tag{8}$$

The integral term of the previous equation can be numerically computed, such as α can be simply obtained by:

$$\alpha^{est} = -\frac{\delta t_i}{\int_{\Gamma_i} \frac{\Psi_1(z)}{c_0(z)^2} d\Gamma} \quad . \tag{9}$$

b. Inversion of the second mode

After the inversion of the first mode, the second step of the inversion procedure is to find β by a usual matched field approach. Setting α to its estimated value, the impulse response of the medium is for a set of M possible value of the second coefficient β. The first spike is extracted on each impulse response. Then, of synthetic data set

$$\left\{ A_i^{\alpha^{est}}, i = 1, M \right\}$$ is available. The same extraction is done for each real sequence.

The final estimate is obtained by a simple correlation:

$$\beta = \arg\min\left(\frac{A^{obs^T} A_i^{\alpha^{est}}}{\left\| A^{obs} \right\| \left\| A_i^{\alpha^{est}} \right\|}\right), (i = 1, M) . \tag{10}$$

where the normalization of each sequence consists in dividing the sequence by its total energy.

4.3. PRELIMINARY RESULTS

The preliminary results of the acoustic inversion on the deepest hydrophone are presented in Figure 10 and Figure 11. Comparisons are drawn with the temporal series of sound speed profiles obtained from the thermistor chain. The global fluctuations of the sound speed field are very well retrieved from the acoustic inversion. In particular, the two minima in the thermocline position are well estimated, which corresponds to the M2 frequency. The magnitude of the vertical displacement of the thermocline is also well estimated and can attain +/- 20 meters around a mean value of 40 meters. On the north station only a small phase delay between hydrology and acoustic can be observed. On the west station this delay is more significant and is estimated to be 0.06 days (1.45 hours). This is reasonable since the direction of the tide is almost perpendicular to the slope.

4.4. DISCUSSION

More work is needed on the inversion in order to be able to conclude on the possibility of retrieving the main characteristics of the tide. This work is in progress. However, the preliminary results shown here illustrate the effectiveness of acoustics to invert for the direction, wavelength and amplitude of the tidal wave. It is important to note that the method does not require heavy nor complicated processing tools, which makes it computationally very fast. It must also be noted that only differential travel times and normalized amplitudes are used. No absolute timing, no precise positionning and no calibrated source are needed. However, the fluctuation in time of the last arrival are only of a few milliseconds and it is therefore necessary to have a signal sampling less than 1 millisecond.

5. Conclusion

This paper has presented an overview of the INTIMATE96 experiment, which aimed to tomographically image internal tides in a shallow water area on the Portuguese shelf. The experiments mainly consisted in acoustic stations north and west from a light 4-hydrophones vertical array. The central result of acoustic data processing is that several effects of the environment, including bottom influence, source range and depth and of course internal tide effects, can be clearly seen on the signals and they can be processed separately. The effect of tides makes inversion possible with simple and fast methods.
INTIMATE96 confirms the efficiency of broadband analysis using simple devices (single hydrophones or light vertical arrays) to infer the geophysical environment. Several studies, in particular in bottom geoacoutic-parameters assessment [21] and source tracking [22, 23, 24], have lead to the same conclusion. In the future, some complementary analysis of INTIMATE96 data inversion will be done and precise comparisons with the hydrology will be drawn.
The second experiment of the INTIMATE series was carried out in the Bay of Biscay in July 98 [25, 26]. Data are being processed but the first result show that in several other types of environment, as sand dunes and rocky areas, broadband signals exhibits the same kind of pattern with in particular stability in the late arrivals. If confirmed, these results would be significant in showing that the analysis of shallow water propagation could extend to most of coastal areas and low frequency active broadband processing could emerge as a robust tool for shallow-water environmental assessment.

References

1. C. Wunsch, "Internal tides in the ocean", *Review of Geophysics and Space Physics*, **13**, 167-182, (1975).

2. W. Munk, and C. Wunsch, "The Moon, of course …", *Oceanography*, **10**, 3, (1995).

3. N.L. Weinberg, J.G. Clark, and R.P. Flanagan, "Internal tidal influence on deep-ocean acoustic ray propagation*", Journal ofthe Acoustical Society o. America*, **56**(2), 447-458, (1974).

4. W. Munk, B. Zetler, J. Clark, S. Gill, D. Porter, J. Spiesberger, and R. Spindel, "Tidal effects on long-range sound transmission", *Journal of Geophysical Research*, **86**(C7), 6399-6410, (1981).

5 W.H. Munk, P. Worcester, and C. Wunsch, *Ocean Acoustic Tomography*, Cambridge University Press, Cambridge, (1995).

6. B. Dushaw, B. Cornuelle, P. Worcester, B. Howe, and D. Luther, «Barotropic and barotropic tides in the central North Pacific ocean determined from long-range reciprocal acoustical transmissions", *Journal of Physical Oceanography*, **25**, 631-647, (1995).

7 J.F. Lynch, G.G. Gawarkiewics, C.S. Chiu, R. Pickart, J.H. Miller, K.B. Smith, A. Robinson, K. Brink, R. Beardsley, B. Sperry and G. Potty, «Shelfbreak primer- An integrated acoustic and oceanographic study in the middle Atlantic bight», *Shallow Water Acoustics*, R. Zhang and J. Zhou Eds., China Ocean Press, (1997).

8. J.R. Apel, M. Badiey, C.-S. Chiu, S. Finette, R. Headrick, J. Kemp, J.F. Lynch, A. Newhall, M.H. Orr, B.H. Pasewark, D. Tielburger, A. Turgut, K. von der Heydt, and S. Wolf, «An overview of the 1995 SWARM shallow water internal wave acousting scaterring experiment», *IEEE Journal of Oceanic Engineering*, **22**, 3, 465-500, (1997).

9. P. Baines, "On internal tides generation models", *Deep-Sea Research*, **20**, 179-205, (1982).

10. R. Mazé, "Generation and propagation of non linear internal waves induced by the tide over continental slope", *Continental Shelf Research*, **7**, 1079-1104, (1987).

11. T. Gerkema, and T. Zimmerman, "Generation of nonlinear internal tides and solitary waves", *Journal of Physical Oceanography*, **25**, 1081-1094, 1995.

12. A. New, "Internal tidal mixing in the Bay of Biscay", *Deep-Sea Research*, **26**, 5, 691-709, (1988).

13. A. Pichon, and R. Mazé, "Internal tides over a shelf break: Analytical model and observations", *Journal of Physical Oceanography*, **20**, 5, 657-671, (1990).

14. N. Pérenne, and A. Pichon «Effect of barotropic tidal rectification on low frequency circulation near the shelf break in the northern Bay of Biscay», *Journal of Geophysical Research*, 106, C6, 13,489-13,506, (1999).

15. F.R. Martin-Lauzer, Y. Stéphan, and F. Evennou, "Analysis of tomographic signals to retrieve tidal parameters", *Proceedings of the Second European Conference on Underwater Acoustics*, Ed. L. BjØrnØ, European Commission, 1051-1056, (1994).

16. Y. Stéphan, F. Evennou, and F.-R. Martin-Lauzer, «GASTOM90: Acoustic tomography in the Bay of Biscay», *Proceedings of IEEE OCEANS96 Conference*, (1996).

17. X. Démoulin, Y. Stéphan, S. Jesus, E. Coelho and M. Porter, «INTIMATE96: A shallow water experiment devoted to the study of internal tides», *Shallow Water Acoustics*, Zhang & Zhou eds., China Ocean Press, 485-490, (1997).

18. Equipe INTIMATE, «INTIMATE96 data report», *technical report n° 27/EPSHOM/CMO/DE/NP*, SHOM, (1997).

19. M. B. Porter, *The KRAKEN normal mode program*, SACLANT Undersea Research Centre Memorandum (SM-245) / Naval Research Laboratory Mem. Rep. 6920, (1991).

20. Y. Stéphan, X. Démoulin, T. Folégot, S. Jesus, M. Porter and E. Coelho, «Influence de l'environnement sur la propagation acoustique par petits fonds : la campagne de tomographie INTIMATE96», *Technical report n° 18/EPSHOM,CMO/OCA/NP*, SHOM, (1998).

21. J.-P. Hermand, «Broadband geoacoustic inversion in shallow water from waveguide impulse response measurements on a single hydrophone: Theory and experimental results», *IEEE Journal of Ocean Engineering*, **24**, n° 1, 41-66, (1999).

22. S.M. Jesus, M.B. Porter, Y.A. Stéphan, E.Coelho and X. Démoulin, «Broadband source localization with a single hydrophone», *Proceedings of IEEE Oceans'98 conference*, IEEE/OES, 1078-1082, 1998.

23. M.B. Porter, S.M. Jesus, Y.A. Stéphan, E. Coelho and X. Démoulin, «Single phone source tracking in a variable environment», *Proceedings of the 4th European conference on Underwater Acoustics*, A. Phillipi & G.B Canneli Eds., Roma, 575-580, (1998).

24. M.B. Porter, S.M. Jesus, Y.A. Stéphan, X. Démoulin, and E. Coelho, « Tidal effect on source inversion», in this volume.

25. Y. Stéphan, T. Folégot, J.-M. Léculier, X. Démoulin and J. Small «Intinmate98 data report. Part 1: Hydrology», *technical report n° 01/EPSHOM/CMO/OCA/NP*, SHOM, (1999).

26. Y. Stéphan, T. Folégot, J.-M. Léculier, X. Démoulin and J. Small «Intinmate98 data report. Part 2: Acoustics», *technical report n° 48/EPSHOM/CMO/OCA/NP*, SHOM, (1999)
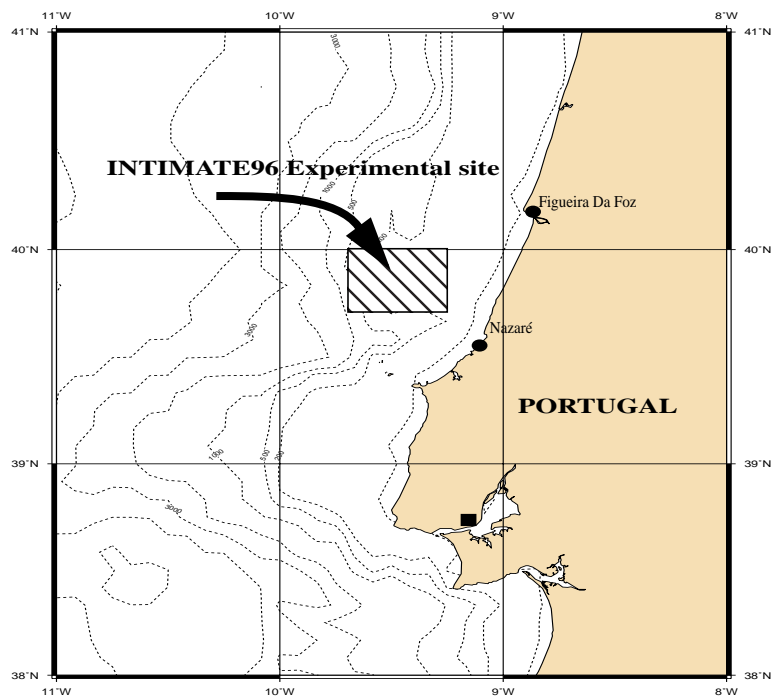
Figure 1: Experimental site of the INTIMATE96 experiment.
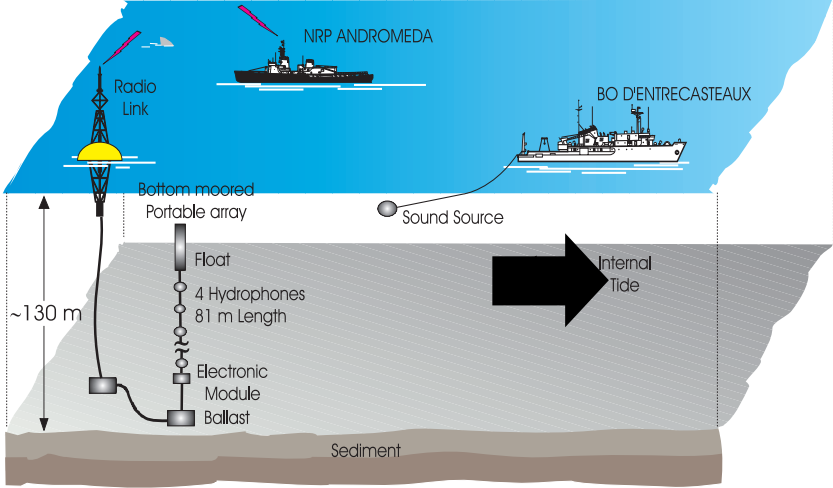
Figure 2: .Experimental set up of the experiment.
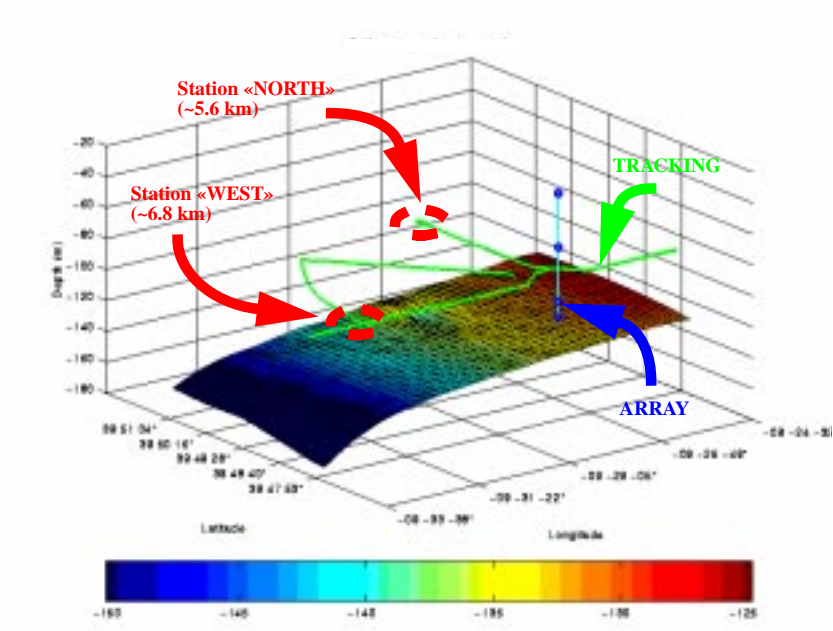
Figure 3: .Description of the phases of acoustic measurements.
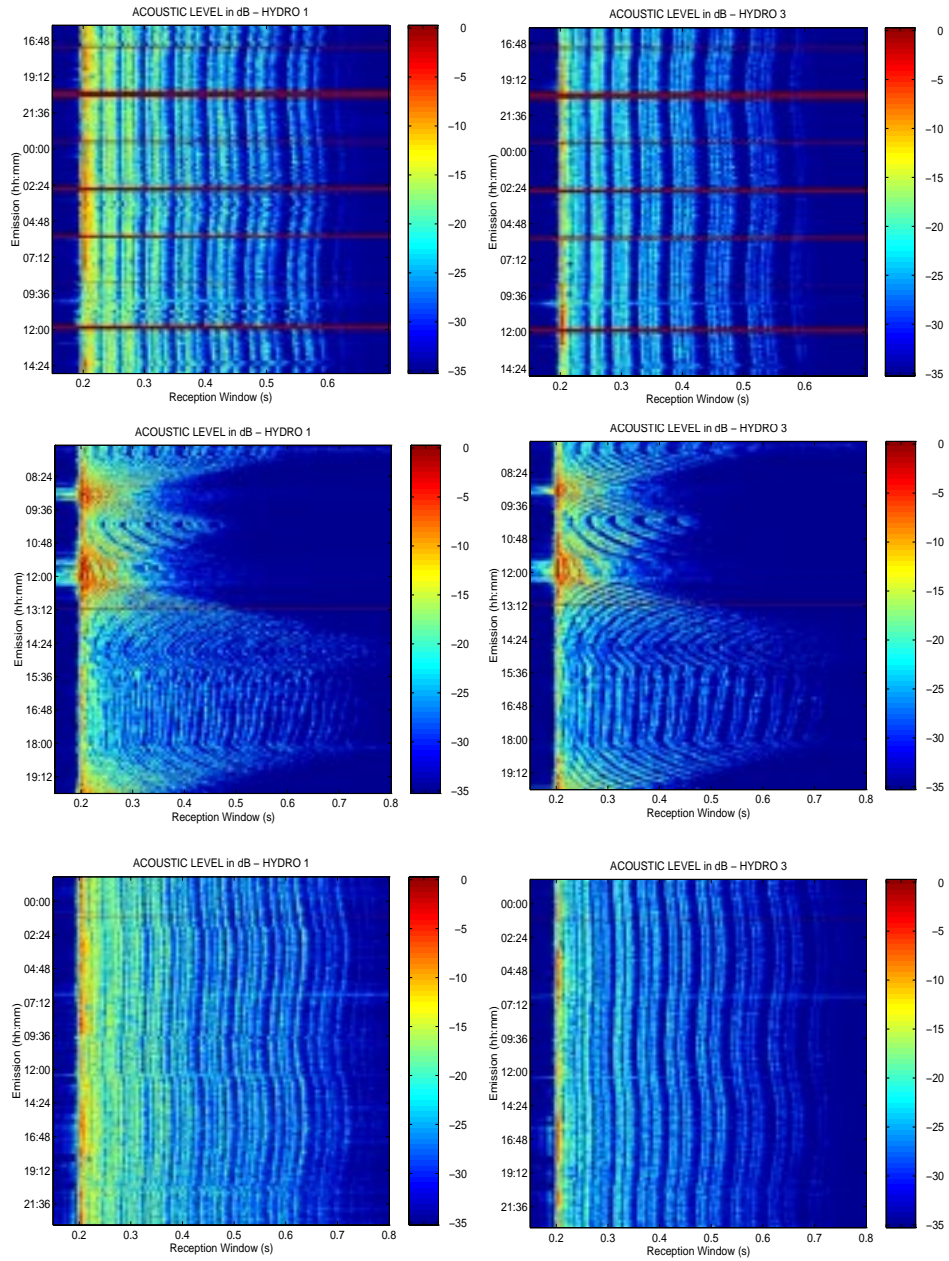
Figure 4: Acoustic data collected on the shallow (left) and deep (right) hydrophone during the station «NORTH» (top), during «TRACKING» (middle) and during station «WEST» (bottom).
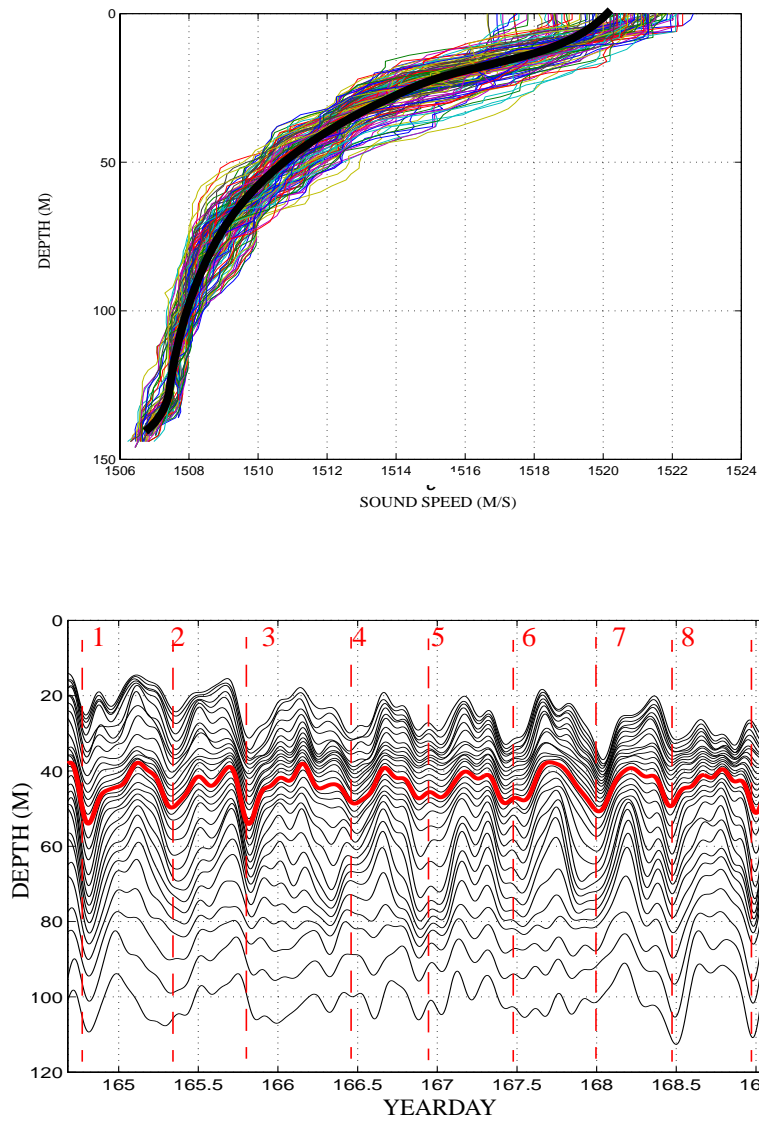
Figure 5: Top: Collection of the CTD profiles measured during the experiment. Bootom: Temperature series near the hydrophone array during 4.5 days. Nine semi diurnal cycles can be seen in the tracking of isotherm T= 16°C.
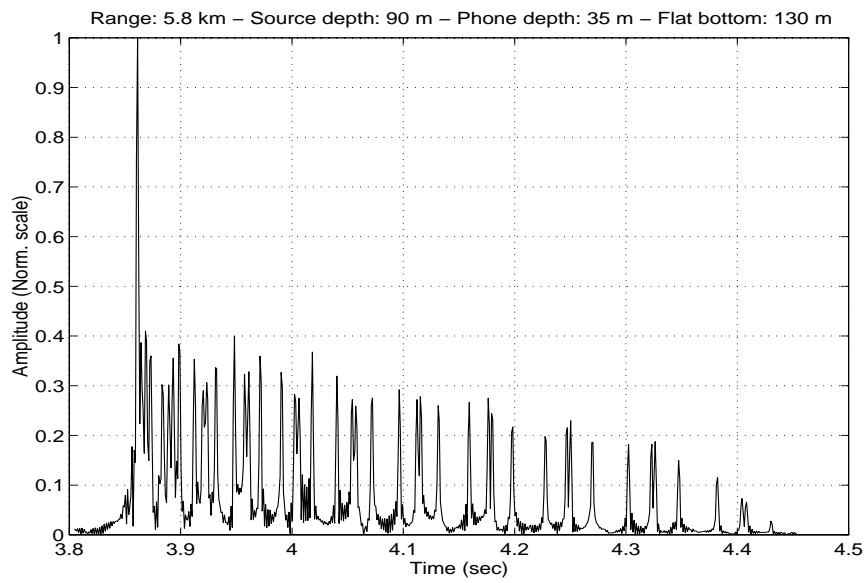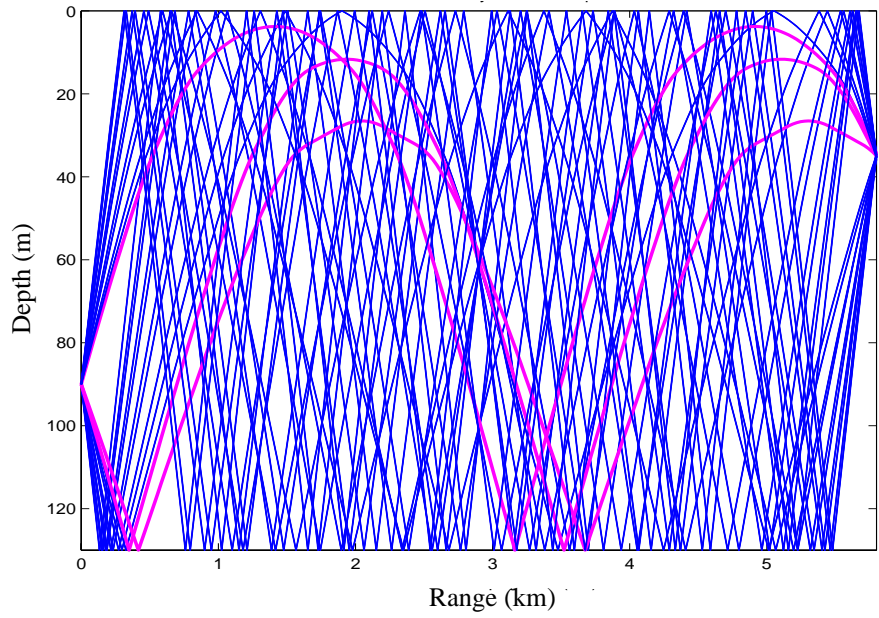
Figure 6: Propagation characteristics in the INTIMATE environment. Top : Ray tracing.
Bottom: Impulse response of the waveguide.
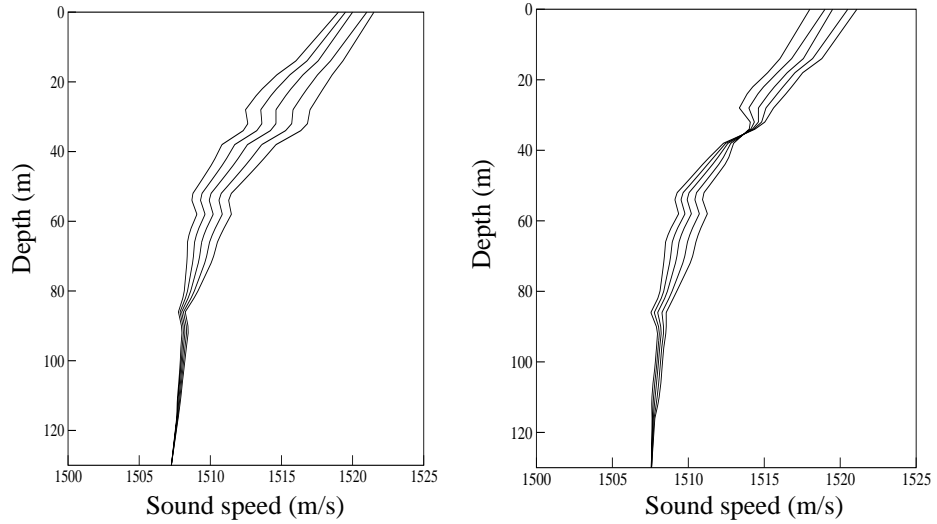
Figure 7: Effects of the two first empirical modes on the sound speed profile. The first mode (left) represents the vertical displacement of the thermocline. The second mode (right) represents the shear in the thermocline.
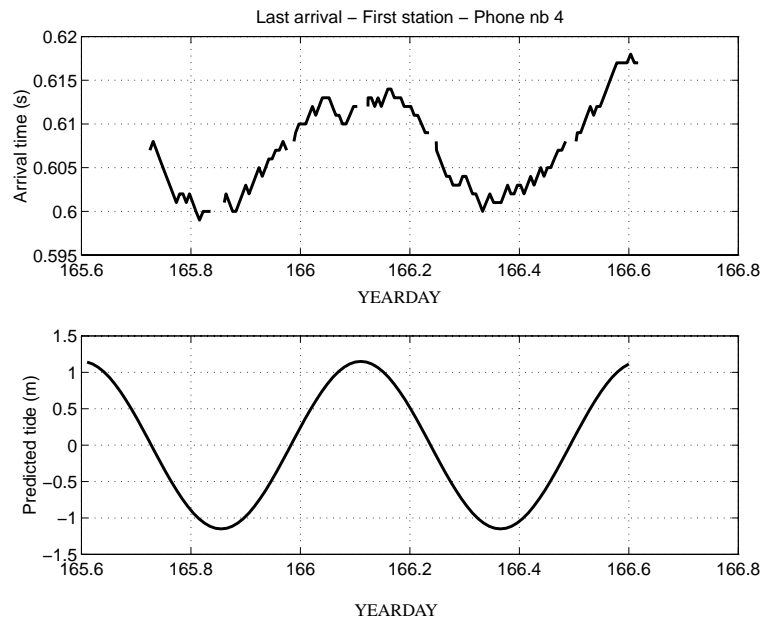
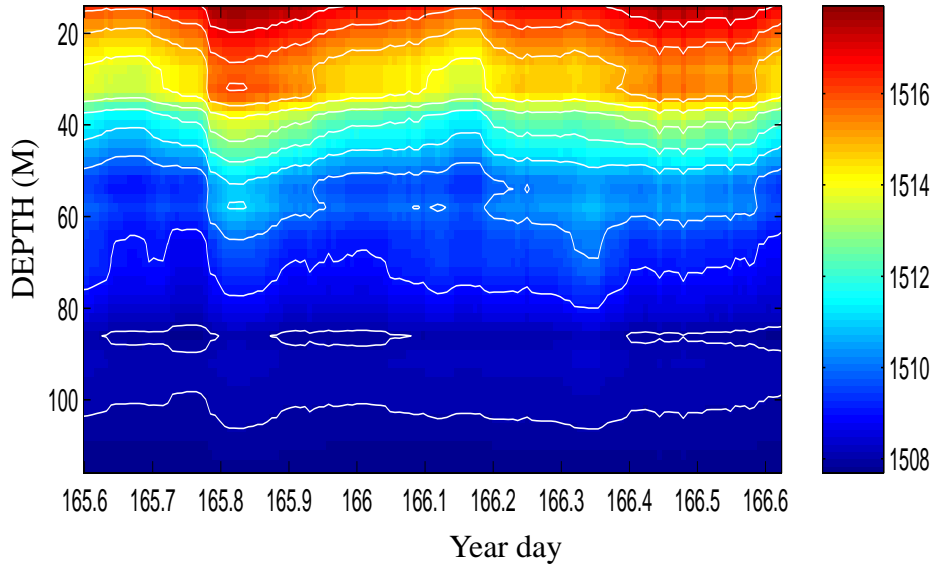**Figure 8: Tracking of the differential travel time of bottom and surface reflected ray during station «NORTH» and comparison with the predicted surface tide.**
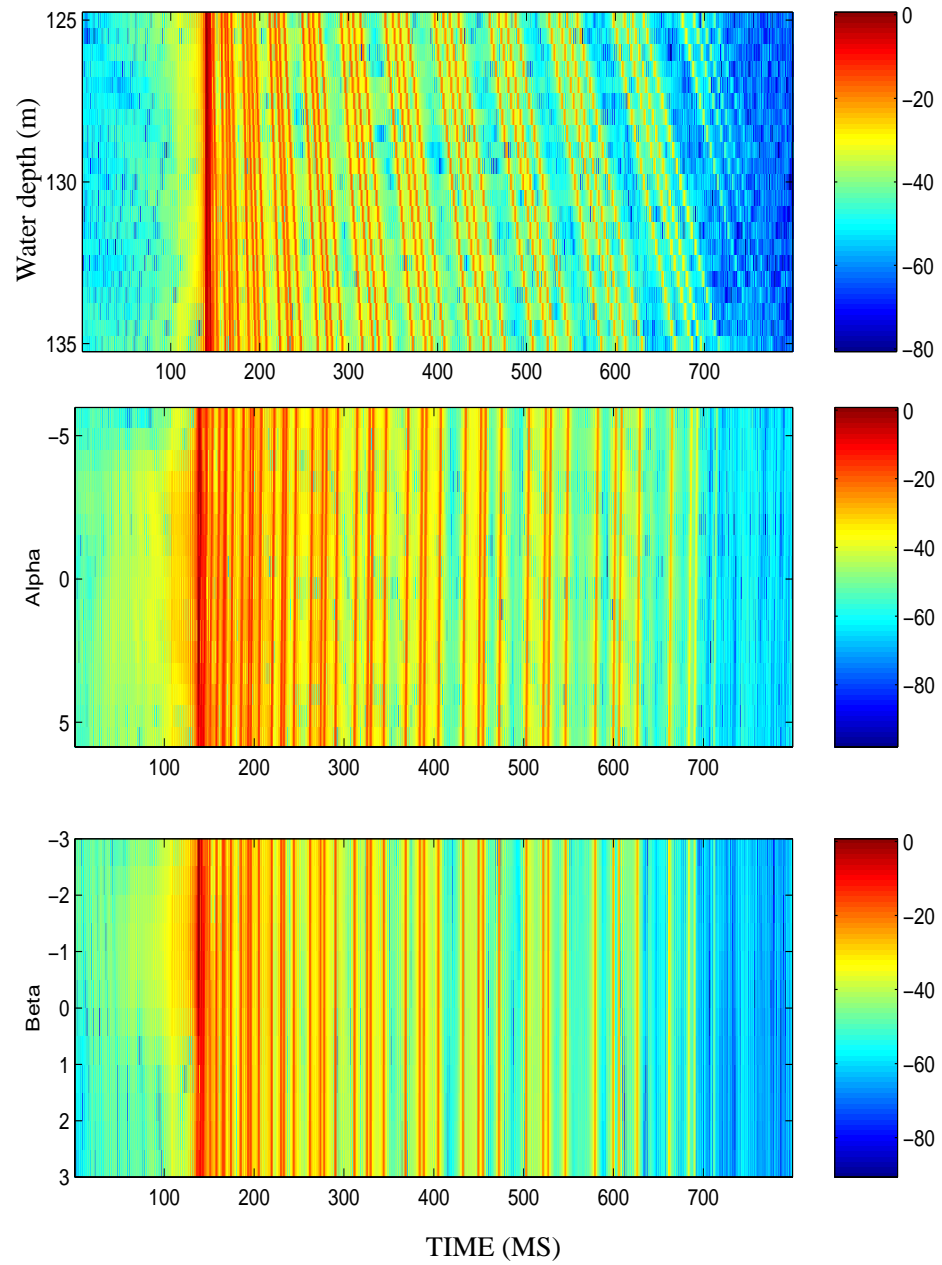
Figure 9: Simulation of the effect of the sea surface (top), the first EOF (middle) and the second EOF (bottom) on the impulse response of the waveguide.

HYDROLOGY
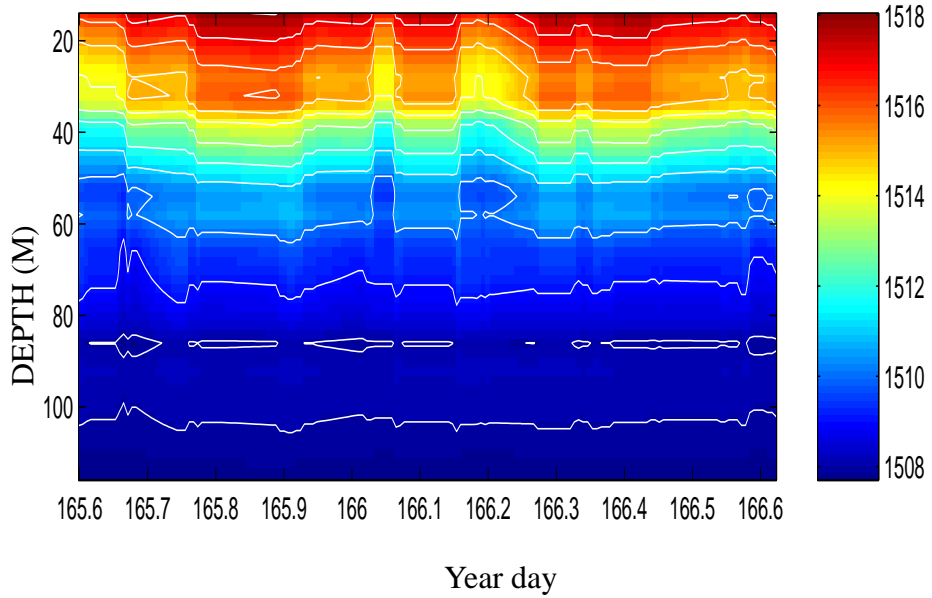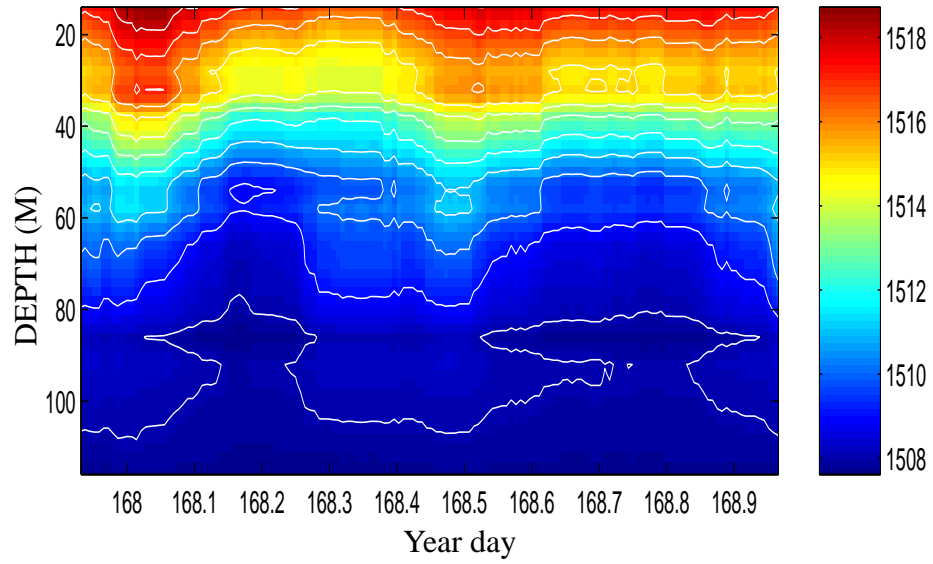

TOMOGRAPHY (hydro 3)

Figure 10: Results of the inversion for station «NORTH» and comparison with the thermistor chain data.
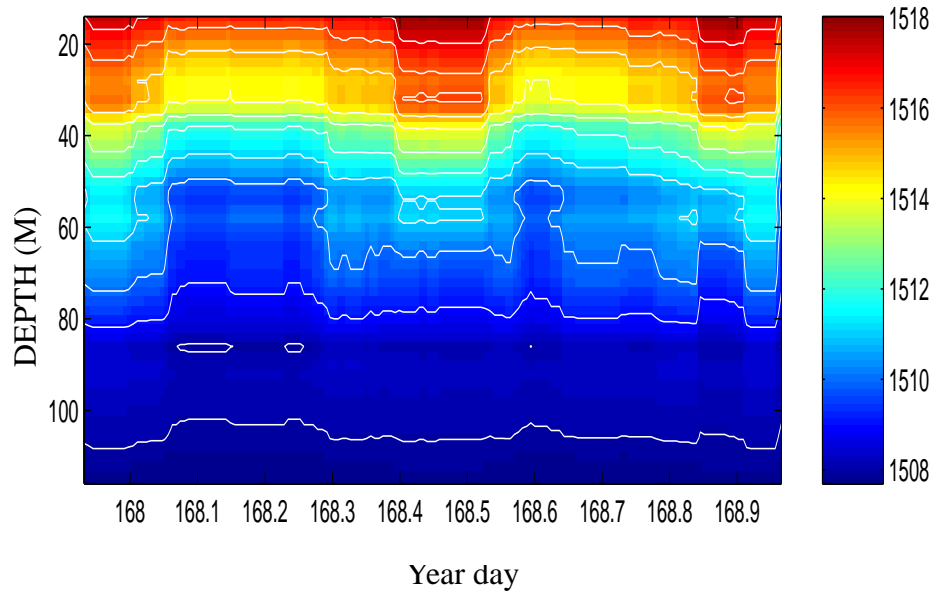
HYDROLOGY

TOMOGRAPHY (hydro 3)

Figure 11: Results of the inversion for station «WEST» and comparison with the thermistor chain data.

ACOUSTICAL EFFECTS OF INTERNAL TIDES

ACOUSTICAL EFFECTS OF INTERNAL TIDES